9

Radio Channel Measurement and Modelling Techniques

Chapter Editor: C. Oestges,
Section Editors: C. Brennan, F. Fuschini, M. L. Jakobsen, S. Salous, C. Schneider and F. Tufvesson

This chapter is dedicated to radio channel measurement and modelling techniques for beyond 4G networks, in particular:

- new measurement techniques not only targeting radio channels, but also material properties in new frequency bands (Section 9.1),
- improved physical models, cowering full-wave as well as ray-based methods, with a specific sub-section dealing with diffuse scattering (DS) and complex surfaces (Section 9.2),
- progress in analytical models (Section 9.3),
- new channel estimation tools for model development based on channel sounding data (Section 9.4), and
- finally, updates on COST 2100 channel models, enabling to include new features such as massive and distributed multiple-input multiple-output (MIMO) aspects (Section 9.5).

9.1 Measurement Techniques and Material Characterisation

Radio noise and channel measurements are fundamental to channel characterisation and system design. While techniques using commercial off the shelf (COTS) such as VNAs offer a ready to use solution they tend to suffer from a slow repetition rate that does not permit capturing the dynamic behaviour of the channel. They also have limited range in particular in the higher frequency bands. VNA measurements can provide reference data and used to develop channel models for indoor environments in out of the office hours. Such measurements have been performed to study the possibility of extrapolating the channel parameters in space and in frequency [Nik12]. Using a three dimensional robot, both single-input multiple-output (SIMO)

Cooperative Radio Communications for Green Smart Environments, 341–382.

and MIMO measurements were performed with 50 MHz bandwidth between 2.45 and 2.5 GHz. In the SIMO measurements, the transmit antenna was fixed while the receiver (RX) antenna was moved in steps of 25 mm to cover a space of 1.5 $\times$ 0.5 $\times$ 0.5 m. The MIMO measurements emulated the downlink and measured the channel over 35 transmitter (TX) locations on a straight line while the RX was moved in the x, z domain over 8 $\times$ 8 locations. Assuming plane wave transmission, the amplitude, phase, and angle-of-arrival can be estimated at a particular location. Using this model, the channel characteristics were extrapolated from one location or frequency to another beyond the 0.5 correlation coefficient for the coherence bandwidth or coherence distance. Using a ray model, the extrapolation distance was extended by more than 0.5λ. The extrapolated channels in frequency were found to improve the beamforming results at separations larger than five times the channel coherence bandwidth.

To overcome the limitations of vector network analysers (VNA) custom designed radio channel sounders are developed. To address the move to the frequency bands above 6 GHz, collocated and distributed multiple antenna technology sounders with modular architecture using multiple frequency bands, and multiple transmit and multiple receive units (MIMO) have been reported in Konishi et al., Stuart and Laly et al. [KKCT12, SFRC15, LGT$^+$15]. The sounder in Konishi et al. [KKCT12] targets the multi-link scenario with a 24 $\times$ 24 MIMO configuration using three transmit units and three receive units with eight channels per unit as illustrated in Figure 9.1. The sounder operates in the 11 GHz band and uses multi-tone transmission to cover a 400-MHz bandwidth giving 2.5 ns time delay resolution. Each TX has

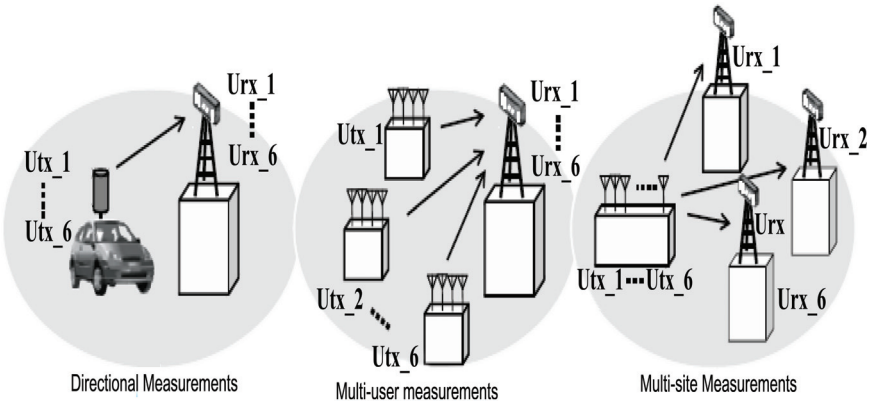

Figure 9.1 Possible measurement variation with scalable architecture.

10 mW per antenna and the RX has 4 GByte of RAM per channel. The overall time delay window is 5.12 μs and the maximum Doppler shift is 3.4 kHz corresponding to a frame length of 146.9 μs.

Using single 10-MHz Cesium clocks at the TX and at the RX for all three units at each site enables time synchronisation. However, the technique is challenging for distributed multi-link characterisation where each unit might require its own reference clock due to the physical separation of the units. Other issues associated with the architecture are the inphase and quadratue imbalance and the impact of phase noise on the estimated channel parameters. These two effects on the multitone signal used in the sounding have been studied in Kim et al. [KKT10, KWS$^+$15]. The impact of phase noise in the local oscillators leads to inter-carrier interference of multi-tone signals. To study its impact on the channel measurements simulations using two models of phase noise were performed. One model represents normal phase noise and has a noise level equal to –62 dBc/Hz, while the second model has high precision phase locked loops with phase noise of –103 dBc/Hz; at 1 kHz from the carrier. The results show that high precision oscillators would be needed for channel measurements and that the effect of phase noise increases as the number of units at the TX and RX increases for MIMO operation. The effect of IQ imbalance is also shown to be reduced by using quarter tone allocation.

To address the multi-tier, multi-band channel measurements, a frequency modulated continuous wave channel sounder with a modular structure (see Figure 9.2(a)) was developed at Durham University [SFRC15, SNCC13, SAG15]. The sounder has five frequency bands with increasing bandwidth as the frequency increases to enhance the resolution of multipath as the wavelength becomes smaller. The bandwidths achievable by the sounder are 750 MHz at 250 MHz–1 GHz and 2.2–2.95 GHz, 1.5 GHz at 4.4–5.9 GHz and 14.5–16 GHz, 3 GHz at 30 GHz and 6 GHz at 58–64 GHz. The sounder enables the configuration of modules as TXs or RXs and for the 30 GHz and 60 GHz bands the RF units are portable to enable on body measurements and avoid loss of cables as shown in Figure 9.2(b). In the mm wave bands, the sounder has an eight by eight MIMO configuration at 30 GHz and a 2×2 in the 60 GHz band which permits the estimation of channel capacity for multiple antenna measurements and for polarisation measurements.

Figure 9.3 shows the difference between the VNA measurements and that obtained with the channel sounder with waveform duration of 819.2 μs. The effect of the long duration of the VNA measurement is seen to distort the channel response in contrast to the clear response obtained with the channel sounder.

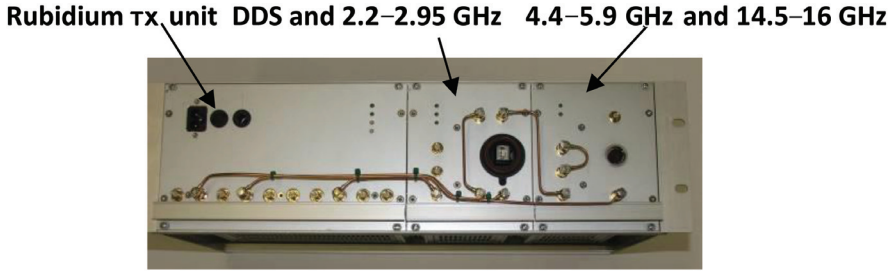

(a)

(b)

Figure 9.2 (a) TX/RX rack housing the three main units. The third unit housing the up converter up to 14.5–16 GHz can be replaced either by TX or RX units for the lower frequency bands and (b) portable 60 GHz units used in on body measurements.

Sounders using PRBS waveforms have been reported by Weile et al. and Hafner et al. [WPKW15, HDMS$^+$15] with chip rates of 250 MHz [WPKW15] or 3.5 GHz [HDMS$^+$15] with carriers at either 60 or 74 GHz, respectively. Using a two channel RX polarimetric measurements are enabled with manually switching the TX antenna [HDMS$^+$15].

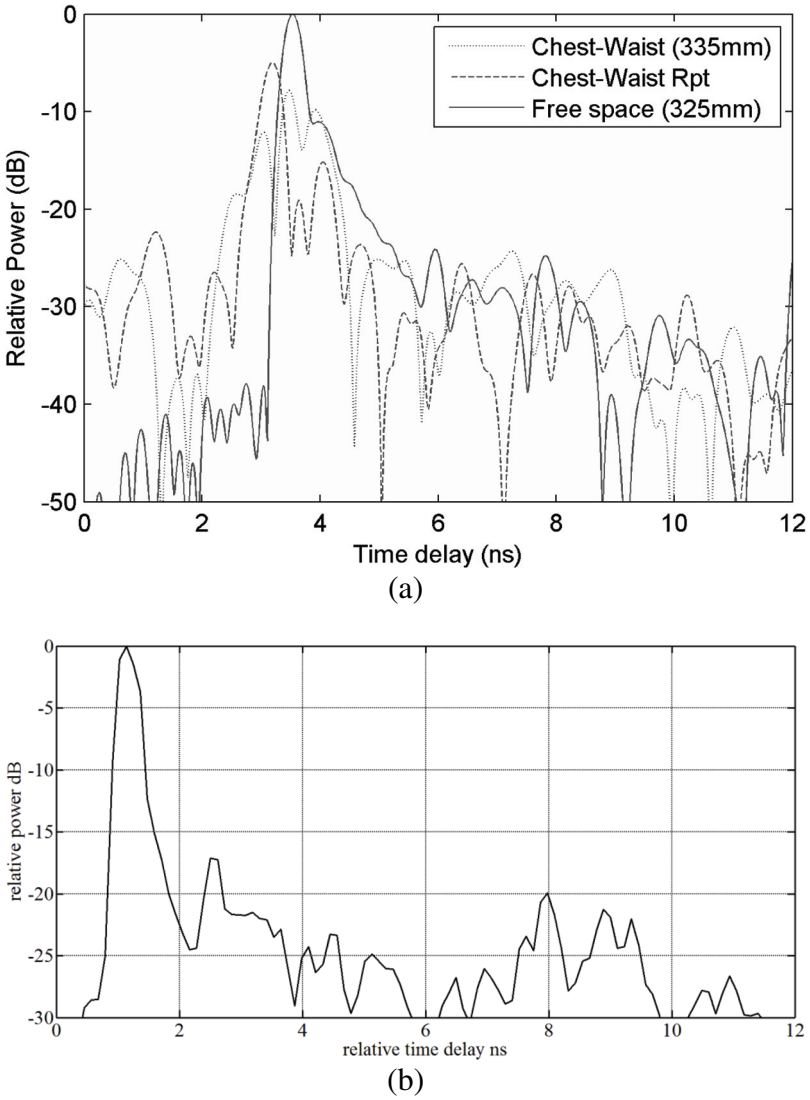

Figure 9.3 On body measurements using (a) VNA and (b) channel sounder.

Two other low cost channel sounders have been reported by Kim et al. and Laly et al. [KWS+15, LGT+15] which use digital techniques and configurable logic to implement either a mm wave sounder at 60 GHz as in Kim et al. [KWS+15] or an 80 MHz sounder at 1.3 GHz for 4×4 configuration [Pie15].

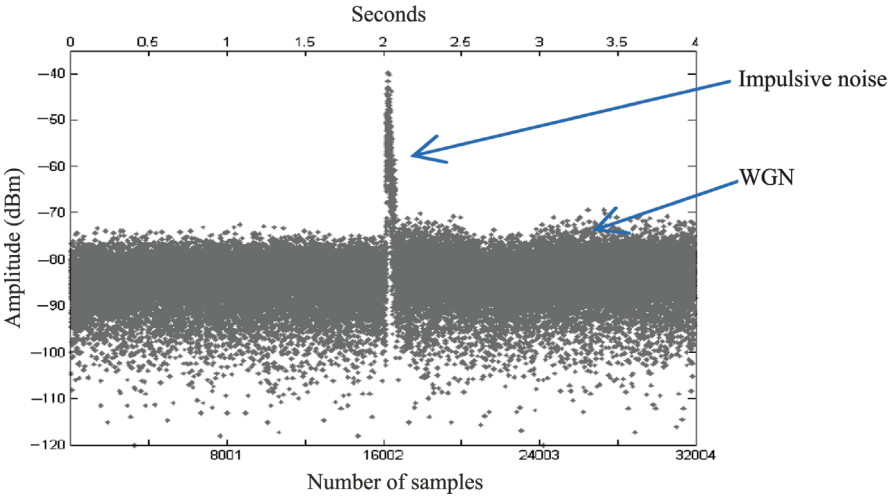

Figure 9.4 Measurement of IN with background WGN.

Another important aspect of radio measurements is that of noise. The presence of additive noise impacts the performance of radio RXs. Noise can be either white Gaussian noise (WGN) or impulsive noise (IN). Noise measurements are performed using an antenna connected to a high sensitivity RX and a programme to control the acquisition of data. To estimate IN, the Gaussian noise is first measured when the source of IN is switched off and subsequently when it is switched on [Mar14]. To capture IN which is short in duration, 8001 samples/s were captured in 4s to obtain the data in Figure 9.4. Parameters representing IN such as the number of bursts, burst amplitude level, burst duration, and burst separation can be evaluated from the data after setting up a threshold of 13 dB above the RMS value of the Gaussian noise as recommended by the international telecommunication union (ITU)-R report SM2155, 2009.

9.2 Physical Modelling Techniques

Radio channel physical modelling is based on the application of a *sound physical theory* to a proper *representation of the environment.* The model is *statistical* if the environment is simply described through few, general parameters; assuming the outdoor urban channel as a reference case, such parameters may be the mean buildings height, the mean street width, etc. On the contrary, if a somehow detailed and specific description of the environment

is needed, the model is said *deterministic* or *site-specific*. Deterministic physical models are mainly addressed in the following.

A deterministic description of the environment refers to both its geometrical and electromagnetic properties. The geometrical description concerns the shape, the dimension and the position of each object inside the environment; these data are often stored into a proper digital *environment database* in vectorial or raster form which feed the model as input file. For a long time, environment databases had to be achieved by hand based on paper maps (e.g., cadastral maps); this procedure was cheap but also rather time consuming and practically limited to restricted environment like the indoor one. The final accuracy was often quite poor due to the lack of details in the starting map. Some automatic procedures have been then established (e.g., aerophotogrammetry), which allow a somehow detailed digitalisation of large areas but are also rather expensive. More recently, detailed digital description and representation of the environment are being more and more available on the web, and proper interface programs may be therefore able to extract the environment database from the on-line maps.

The electromagnetic description requires to associate each object with proper values of the electromagnetic parameters (e.g., relative electrical permittivity ε_{R} and conductivity σ) of the materials it is made of, so that its electromagnetic behaviour (e.g., reflection and transmission coefficients, absorbing properties, etc.) can be defined. Again, such information is often stored in a second input file somehow linked to the environment database. Unfortunately, permittivity and conductivity are little known in several cases, and compound materials are often accounted by means of rough effective electromagnetic parameters. Irrespective of the way they are achieved, both the environment and the electromagnetic databases are always affected by unavoidable imprecisions, which may impact on the model performance to an extent that must be evaluated case by case. In order to partly compensate for performance degradation due to inaccuracies in the environment description, empirical or statistical elements are often embedded into deterministic physical models. If, for example, surface roughness or building details such as windows, balconies, rain pipes, etc., are missing in the urban database, then an empirical/stochastic modelling of scattering generated by those details should be introduced in the deterministic model.

Deterministic physical models may potentially produce a wide spectrum of results, ranging from narrowband to wideband prediction, up to a full multidimensional characterisation of the channel, i.e., related to the polarimetric, space–time distribution of the received signal contributions in a

multipath environment. This represents a valuable quality for the design and the deployment of next wideband, multi-gigabit radio systems. In fact, the effectiveness of multi-antenna technical solutions such as antenna diversity, spatial multiplexing, and beamforming, already included in the 802.11ad and long-term evolution (LTE) standards and seriously considered also for future 5G systems at millimeter-wave [RSZ+13, RSP+14], still depends on the received signal strength but also on others parameters strictly related to the multi-dispersive nature of the radio channel.

Physical channel modelling is commonly based on two main approaches: the full-wave electromagnetic approach and the ray approach. In the former case exact field representations such as Maxwell's equations or other similar analytical formulations are solved through numerical methods (e.g., finite difference time domain (FDTD) or MoMs). In the latter case asymptotic methods corresponding to geometrical optics (GO) and its extension allow for a ray-based representation of radio wave propagation. A further, quite known option is physical optics (PO), which is something in between GO and full electromagnetic formulations.

With respect to statistical and empirical channel models, deterministic channel characterisation allows for a more thorough insight into the propagation phenomenon. Nevertheless, high complexity, heavy computational burden and performance degradation due to lack in databases accuracy represent drawbacks that still need to be improved.

9.2.1 Full-Wave Electromagnetic Models

Full-wave models can be classified as being frequency domain or time domain depending on the form of Maxwell's equations used. These equations are most commonly expressed in the form of coupled differential equations but can also be manipulated into the form of a coupled set of equations involving integrals over volumes and bounding surfaces. Hence approaches can be further classified as being differential equation or integral equation based and the section which follows reviews full-wave electromagnetic modelling work carried out in COST Action IC1004 under these two headings.

9.2.1.1 Integral equation-based methods

There are several integral equation formulations of scattering problems, but in each case the principle is the same. The physical problem of a source radiating in the vicinity of a scatterer or scatterers is replaced with one or more *equivalent problems* where the scatterers have been replaced by a collection of unknown sources (mostly currents but in some cases charge densities). These

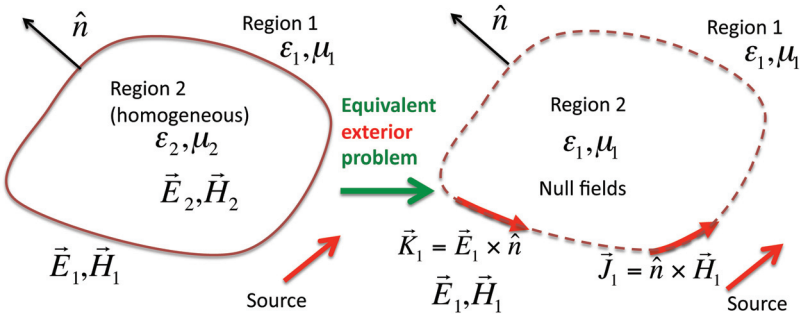

Figure 9.5 Equivalence principle for homogeneous scatterer. The configuration on the right produces the same fields exterior to the scatterer as the physical problem on the left. A similar arrangement is possible to recreate the fields in the scatterer's interior. Applying boundary conditions along the surface results in a set of coupled integral equations.

are assumed to radiate in an unbounded medium, allowing us to use potential integrals to write explicit expressions for the fields. Separate expressions can be thus obtained for fields exterior and interior to the scatterer. Applying boundary conditions along the scatterer surface results in coupled equations for the unknown sources. Figure 9.5 illustrates an example where the physical problem on the left is replaced with an equivalent problem on the right which can reproduce the fields exterior to the scatterer. Depending on the fields one works with it is possible to derive the electric field integral equation (EFIE), magnetic field integral equation (MFIE) or combined field integral equation (CFIE). In addition, one can derive volume integral equations in cases where one is considering inhomogeneous scatterers. In this case the unknown currents are distributed throughout the scatterer volume rather than residing on its surface. A simplified form of the surface EFIE equation holds for the case of perfectly conducting (PEC) scatterers as one only need consider a surface electric current (as the tangential electric field, and thus $\vec{K}$, is zero).

The MoMs [Har93] is used to discretise the integral equation. N basis functions are introduced to describe the unknown currents and charges and these are tested against N testing functions[1]. This results in a $N \times N$ linear system that can be solved using direct or iterative linear algebra methods. As one would expect increasing N generally results in a more accurate solution (albeit at the expense of greater computation times). Van Lil and De Bleser [VLDB14a, VLDB14b] examine the influence of the number and positioning

[1] One could use $M > N$ testing functions, in which case the resultant system would be solved in a least squares sense.

of the basis and testing functions on the accuracy of a method of moments (MoM) solution to a simple 2D problem involving computing the capacitance of a PEC strip. Using a higher density of basis functions at the edges where the charge density varies more rapidly is shown to give better results than a uniform distribution. Using a slightly higher number of testing functions than basis functions results in a rectangular system which can lead to improved accuracy, although this is sensitive to the precise numbers of functions chosen.

Another numerical issue that affects the surface EFIE is the so-called low-frequency breakdown whereby the solution becomes unstable as one approaches zero frequency. The instability is due to the explicit inclusion of charge continuity via the Lorenz gauge which removes the surface charge density as an independent unknown but introduces a $\frac{1}{\omega}$ term which results in a singularity at DC. An alternative is to include the surface charge density as a separate unknown in addition to the surface currents. Such an approach was considered for the case of PEC scatterers in De Bleser et al. [DBVL$^+$11a] and extended to the case of scattering from dielectric scatterers in De Bleser et al. [DBVL$^+$11c]. The extension necessitates the introduction of both electric and magnetic surface charge[2] and the paper outlines the relevant details needed to numerically compute singular integrals etc. Good agreement is obtained for scattered fields at low frequencies indicating the stability of the method. The accuracy of this stabilised method was examined in De Bleser et al. [DBVL$^+$12a, DBVL$^+$11d] by applying it to more complex problems, such as scattering from wind turbine blades, cubes with sharp and rounded edges as well as multi-layered bodies. Further scrutiny is carried out in De Bleser et al. [DBVL$^+$12b, DBVL$^+$11b] wherein quantitative verification against a Mie series solution is provided as is qualitative verification as to whether the boundary conditions are properly satisfied etc. Good agreement is observed at low frequencies as well as a small mesh-dependent error as frequency increases. Further technical detail is provided relating to singularity removal (for the self terms of the impedance matrix) as well the choice of testing and basis functions (including the need to test both tangential and normal components).

While the combined charge and current formulation improves the stability of the method it increases the number of unknowns which has an adverse affect on the computation time. An alternative formulation, referred to as the split formulation, is given in De Bleser et al. [DBVL$^+$13] and [DBVL$^+$14]. In this approach the surface charge is eliminated as an unknown, as in the standard EFIE, but this time without introducing the $\frac{1}{\omega}$ dependency which is

[2]Magnetic charge, while unphysical, is a useful and valid mathematical abstraction.

responsible for the low-frequency instability. The resultant approach is faster and remains stable at low frequencies.

Another key challenge in applying moment–method solutions is their associated computational burden. Discretising an integral equation with N basis and testing functions results in a dense linear system of size $N \times N$. Standard iterative solution using a Krylov solver scheme such as GMRES has computational complexity $\mathcal{O}(N^2)$ due to the necessity to perform at least one matrix vector multiplication at each iteration although various acceleration methods such as the Multilevel Fast Multipole Method (MLFMA; [SLC97]) and spectral acceleration [CJ00] can reduce this burden to something approaching $\mathcal{O}(N \log N)$ which can speed up analysis significantly. Spectral acceleration is used in conjunction with the forward backward method by Brennan et al. [BTM$^+$13] and [BT12] to analyse the fields scattered from randomly rough surfaces. As communication frequencies increase the small random perturbations on a surface become more prominent with respect to the wavelength and the consideration of non-specular or diffuse reflection becomes more significant. The forward backward method is an alternative iteration scheme which sequentially computes the fields along the rough scatterer profile firstly away from the source and then back towards it, implicitly computing all multiple scattering events in a natural fashion as it does so. While less robust than Krylov solvers it has been shown to yield a convergent solution in fewer iterations when applied to certain classes of problem. The work mentioned above includes a novel numerical check to identify when the iteration solution update (i.e. the difference between two successive solution estimates) has broadly converged to a single direction (in the solution space) and, if this is the case, takes an optimised step in this direction. This simple expedient can significantly reduce the number of iterations needed. The method is applicable to TE and TM polarisation and can accurately compute quantities such as the normalised bistatic-scattering coefficient more rapidly than competing full-wave techniques.

More aggressive approximations are required when developing full-wave path loss models for large-scale propagation problems. The fast far field approximation (FAFFA) can yield greater efficiencies at the expense of introducing slightly higher, albeit acceptable and controllable, error and has proven useful for creating 2D propagation models, notably the tabulated interaction method (TIM) which optimises this process for propagation over undulating rural terrain profiles. Extension of such acceleration techniques to more complex propagation problems such as propagation in the vertical plane over the rooftops of buildings poses several challenges such as the effect of sharp edges and the enhanced levels of multiple backward and

forward scattered fields. Brennan et al. [BTD11] and [BT13] address this problem in two ways. First, the FAFFA can be used to reduce the cost of each matrix vector multiplication. Second, a block forward backward method can be used to iterate the solution. The block method is similar to the forward–backward method discussed above but instead conceptually breaks the profile into connected strips (each containing many discretisations) and marches a solution from strip to strip (rather than from discretisation to discretisation) thereby working with blocks of the impedance matrix rather than individual entries. In practice, a hybrid method is used, using blocks of varying sizes—this is referred to as the hybrid forward backward method (HFBM). Results published in Brennan and Trinh [BT14b] (Table 9.1) indicate greater accuracy when predicting path loss for three urban routes in Munich, Germany when compared to SDMs Figure 9.6 for an example).

Table 9.1 Mean (η) and standard deviation (σ) of error between slope diffraction method (SDP), HFBM-FS (forward scattering) and measurements for points far from source such that vertical plane propagation is dominant

	METRO 200		METRO 201		METRO 202	
	η	σ	η	σ	η	σ
HFBM-FS	–1.2	7.3	4.26	7.95	0.57	9.7
SDP (Knife edges)	14.8	8.1	15.6	8.24	14.3	10.1
SDP (Wedges)	–1.1	8.0	–	–	–3.8	10.8

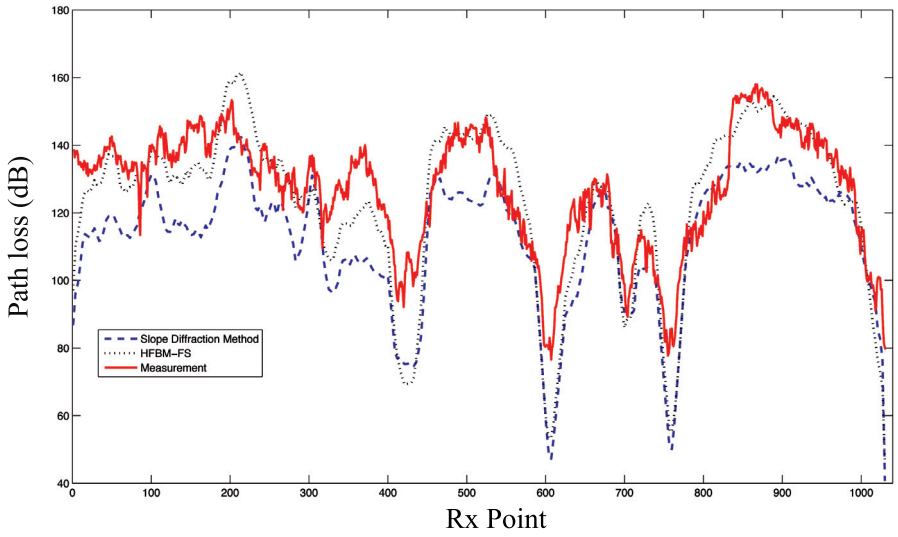

Figure 9.6 Predicted versus measured fields at for the commonly used METRO 202 route in Munich, Germany. Slope diffracted fields assume knife edge buildings.

Another MoM-based 2D path loss model is described in Brennan and Trinh [BK14] and Kavanagh et al. [KPCB15] for the case of indoor propagation. In this work, a volume EFIE (V-EFIE) is used. This requires the discretisation of the entire interior of the building but this is compensated by the resultant ability the use the fast fourier transform (FFT) to reduce the cost of each iteration. In addition the papers outline how the unknowns in free-space, which make up the vast majority of the unknowns, can be effectively removed from the iterative process, as they do not influence the fields elsewhere and are only introduced in order to ensure a regular grid which facilitates use of the FFT. Removing the influence of these non-interacting unknowns further reduces the number of iterations required. The model can include various material types (wood, glass, etc.) and initial validation shows that the model produces shadowing whose characteristics are similar to commonly used statistical models. The model is currently 2D but work is ongoing to extend it to 3D and to develop a wide-band version which can predict other aspects of the radio channel other than path loss.

9.2.1.2 Differential equation-based methods

An alternative starting point for the development of full-wave models is to use Maxwell's equations in differential form. From this a number of models are possible, such as those based on the application of finite elements or finite differencing. The potential of two time domain models for indoor propagation modelling was discussed in Virk et al. [VVW13]. Recognising the need for accurate models to facilitate femto cell design and cognitive radio deployment the paper firstly gives a brief overview of the FDTD method. In particular, the Yee cell discretisation and time-stepping approach is described. The paper also discusses the time domain ParFlow algorithm. This is based on Lattice Boltzmann methods and is related to the transmission line method(TLM).

A multi-resolution frequency domain version of the ParFlow method (MR-FDPF) is applied in Luo et al. [LLV$^+$12a] and [LLV$^+$12b]. Due to computational constraints the simulation is 2D but this is compensated for by way of calibration against measurement which informs the tuning of material parameter values (including an attenuation coefficient for air). The work cited above is specifically concerned with modelling shadow fading and starts by separating the various propagation mechanisms. A simple path loss model is assumed

$$\mathrm{PL}(d) = L(d) + X_\sigma + F, \tag{9.1}$$

where X_σ represents shadow fading while F represents fast fading. The mean path loss $L(d)$ can be further written as

$$L(d) = L_0 + 10n \log_{10} d, \tag{9.2}$$

The document describes how a local mean path loss (comprising mean path loss and shadow fading) can be predicted by averaging power values computed using the ParFlow model over areas of 3.8 λ × 3.8 λ to average out the effects of F. Simple curve fitting techniques can then be used to estimate L_0 and n. The model is verified against data collected by Stanford University in a 16 m × 34 m office space. The fitted path loss exponent n was 1.59, in close agreement to the value of n computed from the measured data (Eq. 1.44). The extracted simulated shadow fading was shown to fit a normal distribution with σ = 5.87 dB (see Figure 9.7) while the value fitted from the measured data was σ = 7.66 dB.

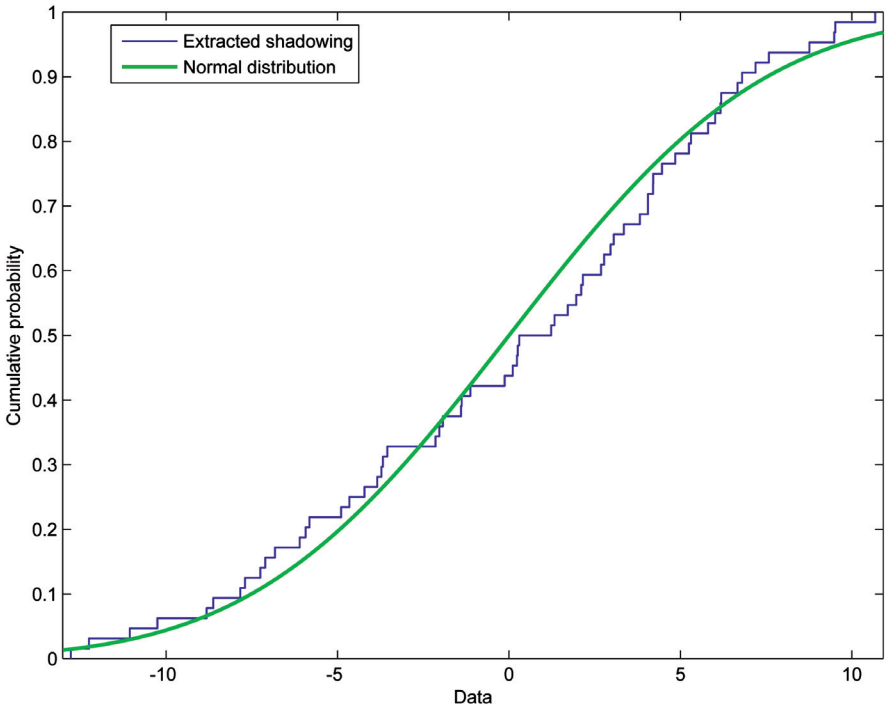

Figure 9.7 Cumulative distribution function of the shadow fading computed using MR-FDPF model (*blue*) versus fitted normal distribution (*green*).

9.2.2 Ray Tracing (RT) Models for Radio Channel Characterisation

Ray-Tracing models are based on the geometrical theory of propagation (GTP), that is an extension of GO to radio frequencies, i.e., not limited to optical frequencies. In order to account for diffraction effects, which can be important at radio frequencies but are completely neglected by GO, GTP includes the so-called uniform theory of diffraction (UTD) [MPM55]. Like GO, GTP is based on the *ray* concept: multipath propagation of electromagnetic waves in real environment is represented by means of rays, that spring out from the TX and may reach the RX after some *interactions* with the objects inside the propagation scenario. Beside standard interactions like specular reflection, transmission and diffraction, RT models have been recently extended to diffuse scattering, which can be important for a reliable multidimensional characterisation of the radio channel [DEFV$^+$07, DDGW03, MQO11, VDEMO13].

Rays trajectories are commonly tracked according to two, different techniques, namely *images RT* and *ray launching* method [IY02].

Since a ray-based description of radio wave propagation somehow corresponds to mental, intuitive visualisation of the actual propagation phenomenon, RT models represent very helpful study and teaching tools. On the contrary, they have not still achieved widespread application to wireless systems design and deployment problems, mainly because of the heavy computational burden and the unavailability of detailed and reliable environment description databases. Moreover, radio system planning has traditionally aimed at pursuing a satisfactory coverage level, and simple, ready-to-use models such as the Hata model [Hat80] have commonly represented a satisfactory and fast solution to achieve the necessary narrowband, path loss predictions.

In the near future things will probably change. As already discussed, RT models are naturally fit to simulate multipath propagation and therefore, to provide the extensive, multidimensional channel characterisation that is necessary to effectively design and deploy the incoming wideband, multigigabit radio systems. Besides, the ongoing idea of accomodating 5G radio networks in the millimeter-wave bands [RSZ$^+$13] may also spur a larger resort to RT simulations, since the smaller the wavelength the more acceptable the ray-optic approximation and the more accurate the RT results. Finally, the computational effort required by RT simulations will be reduced by the increase in computing capacity, and the access to detailed digitised maps of outdoor and even indoor environments will be also easier and simpler in the

next future. RT models are therefore gaining increasing consideration and their use can be expected to become more common for both research and commercial purposes.

9.2.2.1 RT-assisted multipath tracking

Since the experimental characterisation of radiowave propagation is often expensive and time consuming, many effort have been devoted to the development of reliable field prediction models. In this prospect, once the propagation tool has been validated and/or tuned by means of measured data achieved in some reference cases, it should be used *instead of* measurement to assist the radio network planning phases.

In spite of this rather common view, a different option is also possible, aiming at exploiting prediction capabilities *together with* measurement to provide a thorough characterisation of the radio channel. This is done in Meifang et al. [MST11], where a ray launching tool is combined with channel measurements to identify and track the most likely multipath components. In order to increase efficiency, rays are launched from both TX and RX within a cone centred around the measured angles of departure and arrival; a rays matching procedure is then carried out, i.e., common interactions points are searched among rays launched from TX and RX, in order to get complete rays path. Each ray is then associated with a specific multipath component achieved from measurement (basically comparing the propagation delays). Physical scatterers can be visualised onto the map of the environment, and the interaction points with similar delays and rays intensity can be grouped into clusters, which represent a key concept of geometric–stochastic propagation models.

Another method to find the corresponding multipath contributions between measurement and RT simulation is described in [GvDH11] and consists of the following 5-steps procedure: (i) *clustering*: both simulation and prediction are clustered, i.e., multipath components with similar directions of arrival and delays are grouped together; (ii) *calibration*: different conditions between simulation and measurements are eliminated, e.g., the arbitrary start time of propagation delay in measurements; (iii) *feature generation*: each cluster is associated with a single value of delay, azimuth and elevation, as the average of such values among the multipath components belonging to the cluster; (iv) *matching*: each simulated cluster is associated with a measured cluster (v) *evaluation*: check if the matched clusters; and actually come from the same object in the environment.

In some cases, a measured multipath component may have several matched candidates from theRT tool, as well no matching is found in other cases. This

is due to the unavoidable inaccuracies afflicting the RT simulation, e.g., some lack of details in the environment databases, where small objects belonging to the environmental clutter (such as lampposts) are not included but can play an important role from a propagation perspective.

9.2.2.2 New expedients for RT prediction improvement

Although RT application to radiowave propagation modelling dates back to the early nineties, its full potential is still partly unexpressed. A strong effort has been, therefore, devoted to the enhancement of RT performance, aiming at improving the prediction capabilities and/or reducing computation time. To this regard, a sophisticated but effective method is presented in Gan et al. [GMK+13]; the study basically aims at modelling the indoor multipath propagation channel for a mobile terminal moving over a distance smaller than the wavelength λ. In order to compute the time-variant channel frequency response, a standard RT approach would require to track all the propagation paths at different time samples. The required overall complexity can be reduced through a two-step procedure: (i) since the covered distance is lower than λ, the channel is assumed wide sense stationary, i.e., RT can be performed just at the starting position, (ii) each path is projected on a subspace spanned by two-dimensional discrete prolate spheroidal (DPS) sequences [CKZ+10]. The effectiveness of the DPS-based solution in terms of computational complexity reduction is shown in Figure 9.8.

An important source of inaccuracy affecting RT simulators is represented by the rough, oversimplified description of the electromagnetic properties of the materials. Electromagnetic parameters such as the electrical permittivity and conductivity are known only for a restricted set of materials and over limited frequency intervals. In many cases, real materials are a heterogeneous mixture of different and sometimes unknown components, and an electromagnetic characterisation is not available at all. These uncertainties of course reduce the actual accuracy of a RT prediction. A solution to this problem is discussed in Navaroo [Nav13], where the basic idea is to tune the material parameters to optimal values using some calibration measurements as a reference target.

9.2.3 DS Physical Modelling

It is well known that GTP can reliably model propagation in presence of smooth and homogeneous walls and surfaces, where multipath actually consist just of specular, transmitted and diffracted coherent contributions. Nevertheless, propagation in a real scenario is commonly affected also by the so-called

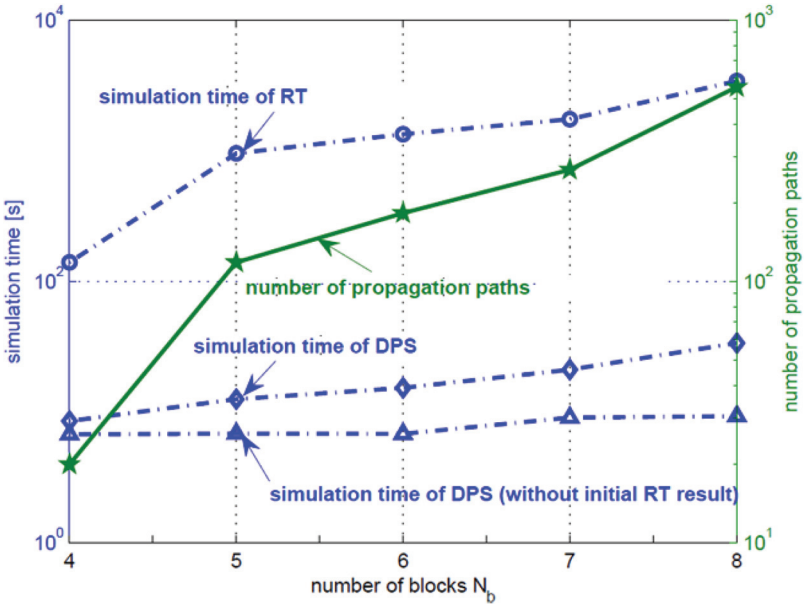

Figure 9.8 Simulation time comparison between standard RT and the DPS approach. N_{b} represents the number of objects inside the scenario.

DS (also known as dense multipath components (DMCs)), that is the result of the superimposition of a large number of incoherent micro-contributions, i.e., with unknown, random phase value an polarisation state. In urban and indoor environment, DS may originate from strong surface irregularities (e.g., windows frames, balconies, rain pipes, etc.) and volume inhomogeneities (e.g., cables and pipes buried inside walls, compound building materials, etc.). Vegetation also represents an important source of scattering, which can be produced by the trees canopy as well as by trunks and branches.

9.2.3.1 Scattering in urban and indoor environment

Owing to its importance for an effective modelling of the multi-dispersive properties of the radio channel, DS from building walls has been recently widely investigated. In Minghini et al. [MDDEV14], the signals scattered by some smooth and rough sandstone slabs placed in an anechoic chamber have been collected and compared in the [2–10] GHz band for different incidence angles of the impinging wave. Results highlight that the field is spatially spread over a wide angular range in the case of rough surface at the expense of the specular reflected component that is attenuated if compared to the smooth slab.

Several models have been then developed to take DS into account, like the effective roughness (ER) model, which has been recently proposed and can be easily embedded into RT conventional tools. According to the ER approach, each wall/object surface is subdivided into small tiles, and the power impinging on each tile is partly reflected specularly and partly scattered according to a proper scattering coefficient S and a specific scattering pattern [DEFV$^+$07]. Both the S value and the width of the scattering lobe should be tuned based on measurement data collected in some reference cases in order to empirically account for the overall scattering effect, since surface irregularities and volume inhomogeneities are usually not included in the input database and a strictly deterministic approach to DS is, therefore, often unpracticable.

The ER model is adopted by Mani et al. [MQO11], where it is embedded in an RT tool to assess the contribution of DS to angular spreads through the comparison between measurement and RT prediction in a laboratory and in an office environment. Measurement have been carried out with a channel sounder working at 3.6 GHZ with a bandwidth of 200 MHz; the receiving antenna was composed of a dual-polarised uniform linear array (ULA), whereas the TX was equipped with a tri-polarised antenna, which was then moved to create a virtual uniform cubic array. Comparison results show that RT with scattering reduces the angle spread prediction error with respect to simulations limited to specular components only. The root mean square error (RMSE) is decreased by 14% for azimuth of departure (AAoD) and 39% for elevation of departure (EoD) in laboratory scenario. Similar results have been achieved for the office scenario.

Although DS is basically an incoherent phenomenon, its depolarisation properties might be not as random as the phase, i.e., the polarisation of the scattered wave could be partly deterministic. The polarimetric properties of diffuse power scattered off building walls is therefore investigated in Vitucci et al. [VMDE$^+$11] by means of broadband measurements carried out at 3.8 GHz along the facades of a rural building and of an office building by means of ULAs of dual-polarised patch antennas at both the link ends. RT simulations including DS according to the ER approach are exploited to extract the DMC from measurements. The specular multipath components, the DMC and the full received signal are then compared in terms of cross-polarisation discrimination (XPD) defined as:

$$\mathrm{XPD} = 10\log_{10}\left[\frac{P_{\mathrm{co}}}{P_{\mathrm{xp}}}\right] \tag{9.3}$$

being P_{co} and P_{xp} the powers received in co- and in cross-polarisation, respectively. Results show that the coherent part of the power generally overestimates the measured XPD, thus highlighting that DS is a key aspect for an accurate prediction of the polarisation behaviour of the channel.

In order to extend the ER model to the polarisation domain, an additional parameter $K_{\mathrm{xpol}} \in [0, 1]$ is introduced into the model [VDEM$^+$13]. According to Equation (9.4), K_{xpol} sets the amount of power transferred into the orthogonal polarisation state after a scattering interaction:

$$\mathbf{e}_{\mathrm{s}} = \sqrt{1 - K_{\mathrm{xpol}}} \left\| \mathrm{e}_{\mathrm{s}} \right\| e^{\mathrm{j}\chi 1} \, \hat{\mathrm{i}}_{\mathrm{co}} + \sqrt{K_{\mathrm{xpol}}} \left\| \mathrm{e}_{\mathrm{s}} \right\| \hat{\mathrm{i}}_{\mathrm{xp}}, \tag{9.4}$$

where $\hat{\mathbf{i}}_{\mathrm{co}}$ is a unit vector representing the polarisation of the scattered field if it were a non-depolarising interaction like specular reflection, and $\hat{\mathrm{i}}_{\mathrm{xp}}$ is the unit vector orthogonal to $\hat{\mathrm{i}}_{\mathrm{co}}$.Comparison between measurement and simulations is exploited in Vitucci et al. [VDEM$^+$13] to tune the K_{xpol} values in different environments; the best-fit K_{xpol} are summarised in Table 9.2 and show that the depolarisation degree of the DMC seems to increase with the complexity of the environment.

In Tian et al. [TDEV$^+$14], a deterministic model for DS is proposed in the framework of the graph theory. If multiple TXs and RXs are considered together with a spatial distribution of scatterers corresponding to the actual shape and position of the objects inside the environment, the channel transfer function is computed through an analytical expression involving several matrices accounting for propagation in line-of-sight (LOS) conditions, from TXs to scatterers, from scatterers to RXs, and among scatterers respectively. The non-zero matrices entries are expressed according to the ER model assuming a Lambertian scattering pattern. It's worth noticing that the matrices to be computed are independent of the number of "bounces" of propagation among the scatterers, i.e., the computation cost is not affected by the number of allowed scattering interactions. The model performance is assessed by

Table 9.2 Best-fit K_{xpol} values in different scenarios

Environment Type	K_{xpol}
Rural building	0.05
Office building	0.2
Campus scenario	0.3
Street-canyon scenario	0.3
Indoor office scenario	0.5
Indoor lab scenario	0.55

comparing the simulated power delay profile (PDP) with RT predictions and real channel measurement data (Figure 9.9). With respect to a previous work of Pedersen and Fleury [PF07], where the propagation graph is set up assuming a random distribution of the scatterers, the deterministic approach generates the PDPs with more realistic decaying slopes. Results are also in good agreement with a RT prediction, provided that the same lambertian model is implemented.

Based on the observation and the analyses of previous studies, DS from real building walls is broken down in Ait-Ighil et al. [AIPFL+12] into three different propagation phenomena, namely specular reflection, backscattering and incoherent scattering (Figure 9.10). Based on a fast formulation of PO [Bal89], a pre-calculated form of GO and five different types of rough surfaces [RBSK70], the three scattering contributions can be computed and combined into the three component models (3CMs), which has been checked against MoM as a reference tool for a complex, isolated building. Results show that the total scattered power calculated using the 3CM approach are in good agreement with the MoM prediction (note that other simulations have been performed using an asymptotic tool and differences with respect to the MoM-based results are similar).

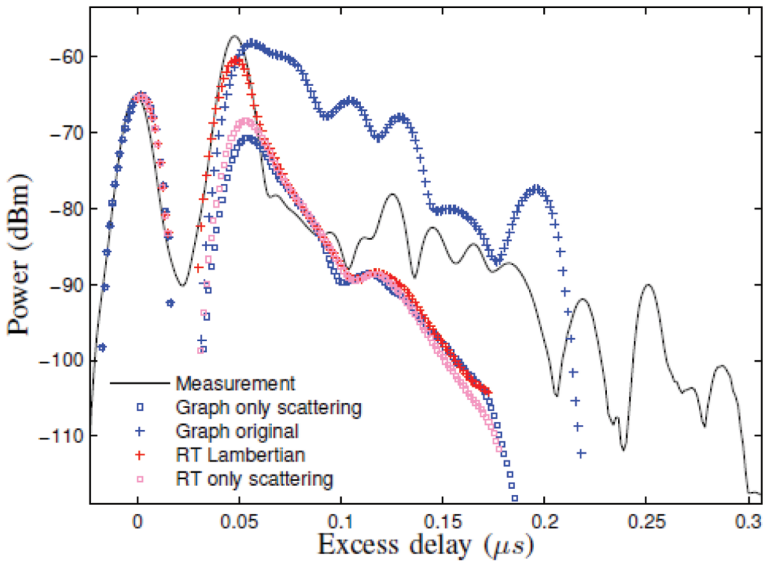

Figure 9.9 Comparison between measurement and different prediction models: deterministic graph model (Graph only scattering), stochastic graph model (Graph original), RT with lambertian scattering pattern (RT lambertian), RT limited to only lambertian scattering (RT only scattering).

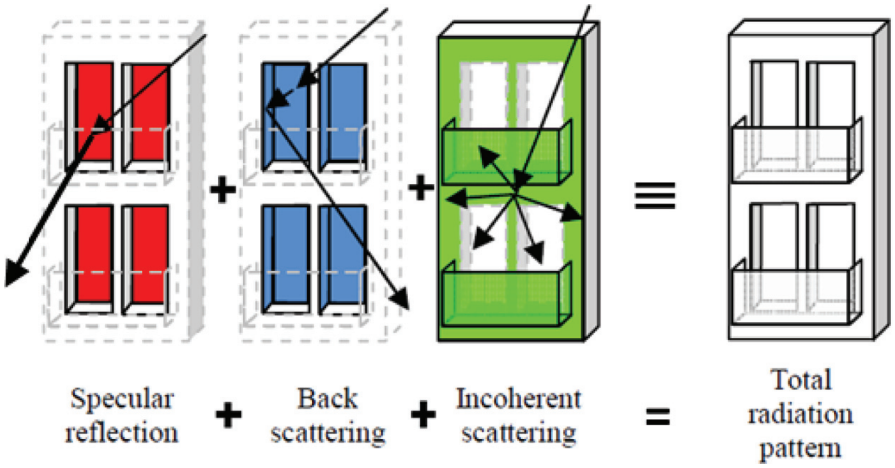

Figure 9.10 Decomposition of the scattering pattern of a complex building.

9.2.3.2 Scattering from vegetation

An electromagnetic wave propagating through a vegetated area undergoes a twofold effect: in addition to the attenuation of the main, forward coherent component, power is also scattered in all the directions (incoherent component). Such effects can be of primary importance in propagation within rural, suburban, or open urban areas.

In Mani and Oestges [MO12], scattering from tree branches is modelled according to a RT approach. Tree branches are modelled as cylinders and a digital representation of a tree is created by means of a 3D-fractal generator. Every time a ray impinges on a tree branch, scattered rays are generated in other-than specular directions. The scattered field is assumed totally depolarised and its overall amplitude is equal to the reflected contribution reduced by a proper coefficient dependent on the angle between the scattered and the specular directions and according to a cosine, linear or exponential law. Comparison with measurement carried out over 15 receiving outdoor locations in a campus scenario shows that the RMSE of the received power decreases from 6.5 to 3.7 dB if scattering from trees is included into the prediction model.

Both the attenuation and the scattering effects due to vegetation are computed in Torrico et al. [TLU13] based on the radiative transport theory applied to a tree trunks dominated environment. The TX and the RX are assumed at the same height and the trunks are represented as identical, circular lossy dielectric cylinders. The intensity of both the coherent and the incoherent contributions to the total received field is computed by means of the 2-D transport equation. According to the result shown in Figure 9.11, the coherent

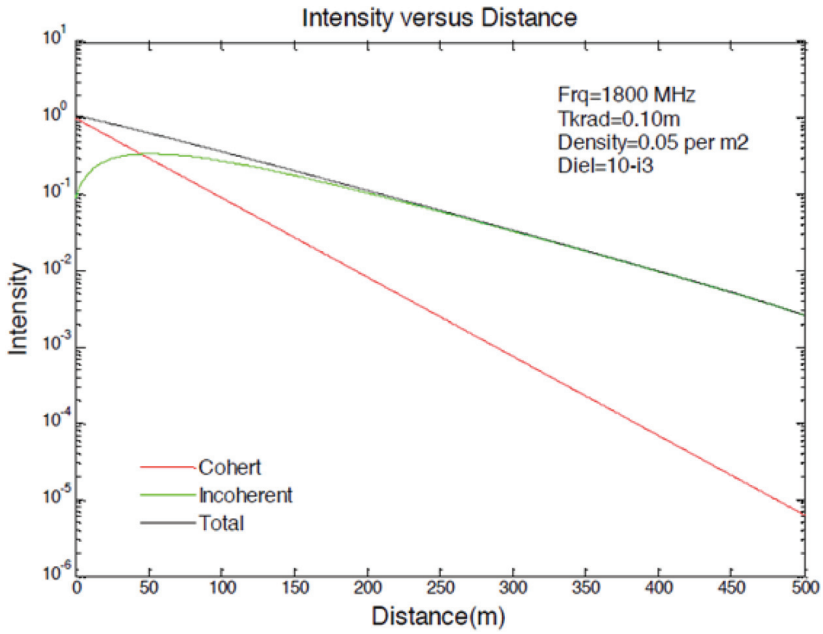

Figure 9.11 Intensities of the received signal contributions versus distance in a trunk dominated environment.

field is dominant only at low penetration distance into the forest layer, where the forward path is affected by few trees; at higher distance multiple scattering effect sets up as the leading propagation mechanism. It's worth mentioning that this behaviour is less evident at lower frequencies and/or for smaller trunks size, i.e., the incoherent waves become increasingly important as frequency and the trunk radius increase.

In Chee et al. [CTK13] the COST-231 Walfisch–Ikegami urban model is extended to vegetated residential environment. Assuming the transmitting antenna elevated above the average rooftop height and separated from the RX by a row of houses and tree canopies, propagation mainly occurs in the vertical plane over the rooftops and through the canopies, and then from the rooftop down to the street level. The theory of Foldy–Lax [Fol45, Lax51] is then exploited to embed scattering and attenuation effects due to the presence of trees into the formulation proposed in the COST-231 Walfisch–Ikegami model for over-rooftop and roof-to-street propagation. At the end, the impact of vegetation on the final, analytical expression for the overall propagation loss is accounted through two main additional parameters, namely the width of the canopy (ω_T) and its specific attenuation (γ). The model

performance are investigated in Chee et al. [CBZ+12], where predictions with and without trees are compared with several cross-seasons measurements carried out at 800, 2300, and 3500 MHz. Results show that the extension to vegetation effects yields significant improvements in moset cases over the COST-231 Walfisch–Ikegami model. Furthermore, the change in the propagation loss due to the seasonal variation in the degree of foliage can be somehow tracked by the model, provided that the canopy-specific attenuation value is properly set for the different seasons.

9.2.4 Other Issues Related to Physical Channel Modelling

Other activities related to deterministic channel modelling have been carried out within the COST IC1004 Action and are addressed in this section. The study in Zentner and Katalinić. [ZK13] and Mataga et al. [MZK13] basically aims at obtaining some scheme for preserving the accuracy of the RT approach, but reducing the the computational effort and the complexity.

The proposed solution is based on the concept of "*ray entity*", that is a group of rays undergoing the same type of propagation interactions, in the same order and on the same object. The space region where the ray entity is present defines its *visibility region.* According to GO basic theory, different rays reflecting on the same walls, i.e., belonging to the same ray entity, appear as originated from a single, fixed virtual transmitter (VTX), whose position corresponds to the multiple-reflected image of the actual TX with respect to the reflecting walls. RT simulations can be, therefore, run with a limited number of RXs, thus reducing the computational burden; then, the results within each visibility region can be interpolated to a higher resolution degree exploiting the ray entity concept at a negligible increase of the computational effort. This opportunity can be also extended to RT simulations including diffraction and DS.

The different strategies to handle VTX position in diffracted rays are investigated in Zentner et al. [ZKD12] with reference to the mobile multipath environment, where Doppler shifts need to be estimated in order to assess the channel temporal variability. With reference to single diffraction for the sake of simplicity, the virtual source is often assumed on the corner edges of buildings, i.e., coincident with the diffraction interaction point. A second option for the VTX position is a point in the ray's direction of arrival, as seen by the user, at a distance corresponding to the total, unfolded path length from the TX to the user. Although they may appear equivalent, the two solutions lead to different values for the Doppler shift related to propagation along the

diffracted ray. In particular, a wrong evaluation is achieved when assuming the virtual source on the diffracting edge.

Diffraction problems are also addressed in Martinez-Ingles et al. [MRMP+12], where an hybrid UTD-PO formulation for the evaluation of multiple-diffraction effects over an array of obstacles is proposed and validated against measurement carried out at 62 GHz. With respect to previous studies, mainly related to the urban propagation context where obstacles (buildings) are usually modelled as knife edges [XB92] or wedges [JLR02], rectangular shapes are considered for the diffracting elements, which could be more appropriate in many cases. The solid agreement between predicted and measured values of the excess attenuation with respect to free space shown in Figure 9.12 corroborates the effectiveness of the UTD-PO solution for the study of wireless communication in the millimetre-wave band. Moreover, since the array of rectangular blocks used during the measurement campaign can be assumed to some extent a scaled-model of an urban environment, the proposed UTD-PO formulation can be also fit to model urban radiowave propagation.

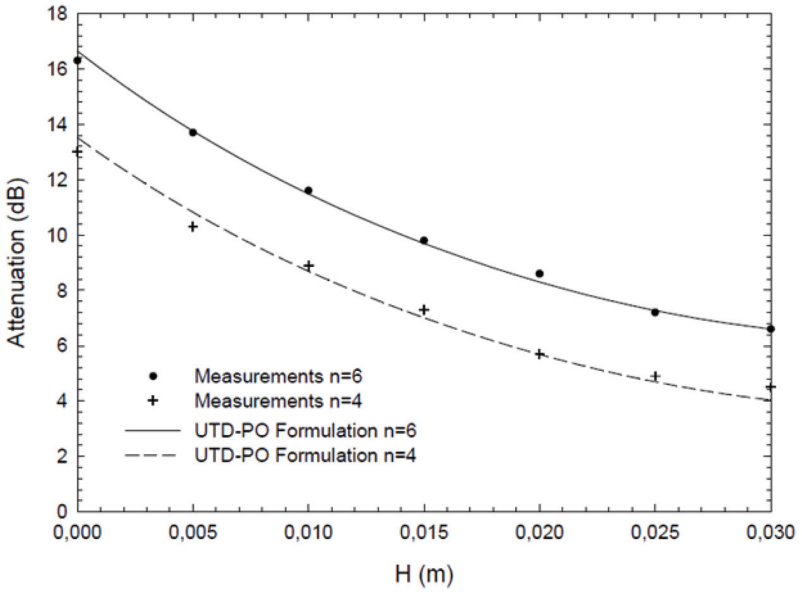

Figure 9.12 Comparison of the UTD-PO prediction with measurements at 62 GHz. H is the relative height of the TX with respect to the array of rectangular obstacles and n is the number of obstacles. Hard/vertical polarisation is considered.

9.3 Analytical Modelling Approaches

Opposite to the physical modelling techniques in the previous section, the present section deals with so-called analytical models. In this terminology, the notion of an "analytical" model carries essentially the meaning of a "non-physical" model. The common approach is to deliberately abandon the physics of electromagnetic wave propagation and to rely instead on conceptually and mathematically convenient simplifications. Thus, the goal is not to accurately reflect the physical processes taking place in the radio channel. Rather, the goal is to design (very) simplified models capable of reproducing and predicting dedicated physical phenomena which can be measured in practice. Modelling designs of this spirit are in the literature often encountered as so-called statistical or stochastic radio channel models.

9.3.1 A Statistical Model of Signal Strength Variability

The statistical model in Giménez [GGGC12] serves as a first illustrative example of an analytical model. Received signal strength is a frequency-dependent quantity in general, and the aim has been to design a model capable of revealing potential gains of time–frequency slicing techniques in digital terrestrial television applications. According to the proposed model, the difference in received signal strength at frequencies f_1 and f_2 depends on two distinct terms: A first term (reflecting propagation losses) parameterised to change deterministically with f_1 and f_2 and a second term modelled as a random variable with a standard deviation parameterised to change as a function of the frequency separation f_2–f_1. Overall, this analytical model includes in its design a total of four parameters whose numerical values are fitted/estimated from measurement data using non-linear optimisation techniques.

9.3.2 Stochastic Models in Two Narrowband Studies

In a study concerned with secure key generation in wireless communications, Mazloum et al. [MMS14] proposed a so-called disc of scatterers-based channel model. The main idea is to exploit (for secrecy purposes) the decorrelation of complex-valued channel gains observed by two different terminals separated at distance d in a narrowband channel. One terminal is the intended RX while the other is an eavesdropper. The physical cause for decorrelation of channel gains versus separation distance is not sought to be explained or

justified. To the contrary, decorrelation serves as a premise and is "constructed" in a mathematically convenient way using a channel gain model in which statistically independent omnidirectional point-scatterers are placed uniformly at random on a disc centred around the intended RX. Individually phased and attenuated contributions from the different scatterers are summed up to yield the complex channel gain at a certain geographical location, yielding increasingly decorrelated gains when separated at larger distances. Using this stochastic channel model, different scenarios are then analysed in terms of secrecy, depending on what type of additional knowledge the eavesdropper has about the propagation environment.

Along similar lines as above, and still mainly in the context of narrowband radio channels, Yin et al. [YYC+13] provides a characterisation of channel polarisation-(an)isotropy. A stochastic model of the channel impulse response is formulated in terms of the so-called bidirection-delay-Doppler spread function of the propagation channel between individually polarised transmit and receive antennas. In the narrowband case and under the assumption that the channel is polarisation-isotropic, analytical expressions are derived for the K factor and the delay spread as functions of the TX-RX polarisations. Both quantities are found to be bivariate quadratic in, and to vary continuously with, the TX-RX polarisations $(p_1,\ p_2) \in (0,\ \pi) \times (0,\ \pi)$. From indoor channel measurements it is however found that the theoretical results are violated, i.e., the properties derived under the assumption that the channel is polarisation-isotropic are not supported by the measurement data.

9.3.3 Combining Partial Models into a Unified Propagation Model Using Signal Flow Graphs

In Vainikainen et al. [VVH13] a framework has been proposed for how to combine various partial models into a single (unified) propagation model, e.g., combining signal strength variability and polarisation anisotropy. The proposed framework can be seen as a network of individual propagation elements. These individual elements are combined to form signal flow graphs as known from, e.g., control systems. Thus, the main idea is to use small and simple building blocks to form branches of a signal flow graph describing complicated multi-dimensional connections between TXs and RXs in mobile communications or navigation. A crucial part in the creation of these signal flow graphs is the elimination of propagation elements that do not contribute significantly to the overall power.

9.3.4 Point Processes in Analytical Channel Modelling

In Jakobsen et al. [JPF14a], the theory of spatial point processes has been employed to revisit a particular class of time-variant stochastic radio channel models. Specific for all models in this class is that individual multi-path components are emerging and vanishing in a temporal birth-death alike manner. The suggested point process perspective has proven to be analytically advantageous, among others by circumventing enumeration issues of traditional modelling approaches. Specifically, traditional integer-indexed sums has been replaced by equivalent expressions indexed by points from spatial point processes. In essence, this allows for keeping track of individual path components by use of the same stochastic mechanism which is also generating the temporal birth-death behaviour of the channel. Under facilitating assumptions the time-variant transfer function of the channel is then shown to be wide-sense stationary in both time and frequency (despite the birth-death behaviour of the individual multipath components). The practical importance of being able to analytically characterise such temporal birth-death channel models is clearly evidenced since key parameters enter explicitly in measurable quantities such as the PDP.

Besides its analytical virtues, the point process perspective is also useful for purposes involving computer simulation. In [JPF14b] it is demonstrated how heuristic and approximate simulation guidelines from earlier channel modelling literature can be replaced by exact (i.e. non-approximate) equivalents. In particular, theoretical properties of Poisson point processes play a fundamental role in obtaining exact schemes for initialisation and time-discretisation.

9.3.5 Statistical Models of Antennas: An Overview

Since the transmit and receive antennas are part of the radio channel it seems out of balance to ignore the inherent stochastic nature (imperfect characteristics) of antennas, while spending vast efforts in investigating and modelling radio wave propagation by itself. Statistical modelling approaches are traditionally uncommon in antenna designs, but this need not necessarily be the case in the future since the current trend is that antennas become more and more complex and hence intuition and experience renders less useful in practice. Quite a lot of scientific work have recently been carried out in the area of statistical antenna modelling. This is evident from the overview provided in [Sib13] along with the list of references therein. One major challenge is argued to be with demonstrating an overall benefit of using statistical modelling

approaches compared to current antenna modelling traditions. It is suggested that the most direct way of getting statistical antenna models to be used in practice is to incorporate them, possibly combined with propagation models, into wireless communication standards.

9.4 Parameter Estimation Techniques

The estimation of channel parameters plays an essential role in bridging the more practical oriented channel sounding task and channel modelling. Channel parameters to be derived from the gathered data sets are well connected to the channel models discussed within the subsequent sections. Within this section three main contributions in the field of parameter estimation can be distinguished:

1. Estimation of basic parameters as fading distributions, spatial degrees of freedom or from the Delta-K model.
2. Estimation of specular and dense multipath parameters which are subject to a defined data structure based on the understanding of the propagation phenomenas.
3. Estimation of multipath clusters and their parameters based on the results of high-resolution multipath parameter estimations.

9.4.1 Estimation of Basic Channel Parameter

Among various channel parameters the fundamental ones are the path loss and fading statistics. Both parameters are important for a proper system design since the outage performance depends on it. Fading basically arises from the superposition of multiple propagation paths (fast fading) and from the interaction of obstacles (shadow fading) as buildings, trees, and so on. The analysis results and interpretation of it depends on the proper definition of analysis methods. A traditional way to analyse the path loss and mitigate the fading is to average over a certain region in space/time conform to the wide-sense stationarity assumption. In Bühler et al. [BZG14] this approach is questioned since the arithmetic mean in the sense of averaging is not robust against outliers and noisy samples. It is proposed to consider the median (e.g., at 50% percentiles) as a more robust estimator. Furthermore the authors proposed not to ignore samples close to or below the noise floor. The results at their selected examples showed that the estimation of the fading statistics based on the two proposals is more robust and reliable.

Another fundamental channel parameter or characteristics is the spatial degree-of-freedom (DoF) since it allows insight to the maximum number of antenna elements in a given volume which optimally support the spatial diversity and multiplexing. In Haneda et al. [HKD+13] an estimation method of the spatial DoF is presented. The proposed concept is based on the spherical wavemode expansion of a radiated electromagnetic field in a MISO configuration and has been verified inside an anechoic chamber before measurements have been performed in an realistic indoor lab scenario. The results show that the spatial DoF is increasing if the size of volume (aperture) and/or the carrier frequency increases. Whereby under LoS condition the increasing volume is not that effective as under NLoS or OLoS. Finally based on the solid angle an antenna-independent metric of the multipath diversity has been introduced. Together with the antenna aperture size the solid angle gives an upper bound of the spatial DoF within the wireless propagation channel.

A different view point into the stochastic radio channel modelling is approached by Jakobsen [Jak14]. The discussion is based on Suzuki's Delta-K model which was proposed to render with a flexible stochastic mechanism the observed grouping (clustering) of multipath components, whereby the renewal Poisson point processes plays an important role. Based on the explicit expression of the log-likelihood function derived in [Jak14] a joint maximum-likelihood estimator for the three parameters of the Delta-K model could be derived. The authors argue the results are promising in the perspective that based on the analytical description and available tools the research on stochastic radio channel modelling could attract again more interest.

9.4.2 Estimation of Specular and Dense Multipath Parameters

It is commonly understood that high-resolution multipath parameter estimation is based on a structured data model comprising two conceptional different contributions: SC and DMCs. The reliability of the estimated parameters depends on the accuracy of the considered data model, used antenna arrays as well as the estimation method. Within that scope several aspects have been discussed.

In Käske [Kä11], the influence of spectral windowing on the estimation results of the DMC is studied. It is known that window functions play an important role in signal processing and estimation, where in practical applications typically only a limited number of data samples are available. In particular in the case of high signal power/high dynamic range of the data the estimation of weaker contributions can be affected by sidelobes

of the window function. It is shown in Käske [Kä11] that using a Hann window instead of a rectangular one increases the estimation accuracy of the noise variance, while the accuracy of the peak value of the DMC is slightly decreased.

Another interesting aspect in high-resolution multipath parameter estimation is the usage of the complex beam pattern. Both contributions [ST13b] and [ST13a] address this, where in Skoblikov and Thomä [ST13b], the impact of a selected elevation cut; and in Skoblikov and Thomä [ST13a], the polarimetric quaternion effective aperture function are discussed. If a uniform linear antenna array (ULA) is considered during the channel sounding and subsequent high-resolution parameter estimation step it is important to know that the estimation results are limited by the geometry of the array: methods based on ULAs (oriented in azimuth) are not able to estimate parameters in the elevation domain. Hence, a fixed elevation angle is often used assuming that all multipath components impinge on the array under that angle. However in practical situations this can not be meet. To discuss the consequences the ambiguity cone is introduced in Skoblikov and Thomä [ST13b]. It basically comprises the effect that multiple azimuth and elevation pairs/combinations will lead to the same phase pattern (measurement result) along a ULA. Subsequently, the estimation results get biased and the variance of the multipath model parameter is increased. In the case that the multipath components occur only in azimuth with common elevation (other cases are also possible, if the ULA is appropriate oriented) the selection of the corresponding elevation cut is necessary. If the selected cut differs from the common propagation elevation again the estimation results in azimuth undergo a bias and increased variance. Both lead to an increased non-realistic spread of the multipath propagation in the spatial domain.

For reliable high-resolution parameter estimation based on channel sounding data sets with dedicated experimental antenna arrays the full polarimetric complex beam pattern of the antenna arrays is required [ST13a]. Typically, the antenna manifold is measured for a finite grid only. For high-resolution estimation of the spatial multipath parameters a precise pattern interpolation is therefore required. A widely used approach is the effective aperture distribution function (EADF) which provides a compact description with low complexity and computational effort for pattern interpolation as well as for calculation of their derivatives (which are necessary for gradient-based estimation approaches as RIMAX [Kä11, ST13b, ST13a, TGJ+12]). However, the EADF is not directly designed for polarisation. In Skoblikov and Thomä [ST13a] a polarimetric extension to the Quaternion EADF (QEADF) is

introduced, where both polarisations are described within one mathematical form and the manifold interpolation is done jointly for both.

The performance of different high-resolution multipath parameter estimation algorithms is evaluated in Tanghe et al. [TGJ+12]. Whereby three algorithms: ESPRIT, SAGE and RIMAX are validated in terms of their robustness under channels including different DMC contributions. While the RIMAX accounts for both SC and DMC parts of the wireless channel ESPRIT and SAGE account only for the SC part. The results for different power ratio's between the SC and DMC part show that estimators which do not consider the DMC part in their data model lead to significant increased estimation errors. In a more extensive study [LKT12], a detailed insight into the influence of inaccurate and incomplete data models on the multipath estimation results is given. It is strongly recommend to include both parts SC and DMC into the data model.

Another interesting approach to investigate the reliability of the high-resolution parameter estimation is discussed in Sommerkorn et al. [SKST13]. Estimators like RIMAX [Kï1, ST13b,TGJ+12, LKT12]) provide the variance of each SC for each propagation dimension. These information can be used to analyse the impact of the estimator on system level performance predictions, e.g., on the MIMO channel capacity. This allows for a different view point on the performance uncertainty of the given estimator. The proposed method consists of 4 main steps: multipath estimation by RIMAX, generation of randomly distorted sets of multipath parameter based on the derived estimation variances, channel synthesis to create the channel impulse responses for the final performance evaluation step. It is important to note that the RIMAX estimation can be interpreted as an antenna de-embedding and the channel synthesis as an antenna embedding, whereby the de-embedding is focused on the dedicated measurement antenna arrays and in contrast to that the embedding is rather flexible in considering more practical antenna arrays. Therefore, the performance evaluation is performed based on the embedding of the measurement antenna arrays and on a typical base station antenna array from Kathrein. In particular for the later array with very narrow beam width in elevation it was of interest to understand if small changes at the direction of departures will create small or large variation at the MIMO performance. The results in Sommerkorn et al. [SKST13] are based on a channel sounding data set from an urban macrocell scenario at Berlin, Germany, and in Käske et al. [KSST14] for the same class of scenario a different data set from Cologne, Germany, has been considered. Both contributions highlight that the estimators variance only weakly affects the

MIMO capacity with slightly larger influence for the more practical-oriented antenna array.

In conventional high-resolution multipath estimators [Kï1, ST13b, TGJ+12, LKT12], it is assumed that the signal waveform of the TX is known. However, in Häfner and Thomä. [HT13], an approach is introduced to estimate the radio channel parameters for unkown TX. Whereby the challenging task is to derive an approach which jointly allows to estimate the channel impulse response (aka blind channel estimation) and to estimate the multipath parameters. Two different solutions, the constrained maximum likelihood and the channel cross-correlation cost function, could be derived which are only dependent on the channel parameters. For minimising the cost functions the Levenberg–Marquardt algorithm was applied. Monte-Carlo simulation-based-results showed that both concepts are nicely applicable.

9.4.3 Estimation of Clusters in Multipath Propagation

Well-known channel models as from COST273/2100/IC1004 or SCM/E or the WINNER family assume that the specular multipath components arrive/depart in clusters. Components with similar properties in the different parameter domains are grouped together—as a cluster. The estimation of such clusters as a post processing step of the above discussed high-resolution multipath parameter estimation is a challenging task since standard approaches as e.g., K-means require a reliable initialisation as well as estimation of the model order (number of clusters). The model order estimation can be considered as pre- or post-processing step, whereat in the latter usually many different clustering results are validated by so-called cluster validation indices (CVI). The contribution from Schneider et al. [SIH+14] studies the robustness and performance of different clustering algorithms based on synthetic channel data sets generated by the WINNER channel model. Within the proposed evaluation framework all clustering approaches have to process the same data sets which allows for the derivation of comparable performances. The WINNER model is taken since its data model is similar to the one considered by common high-resolution parameter estimators such as RIMAX and moreover it is easy to adjust it for different number of clusters and cluster sizes. The spatial dimension of a cluster can be controlled by the inner cluster spread in elevation as well as azimuth, whereby for simplicity only the inner azimuth spread of arrival was changed. In Schneider et al. [SIH+14] two different clustering concepts are compared: the K-power-means and a new hierarchical Multi-Reference Detection of Maximum Separation (MR-DMS).

Within both approaches the selection of the final clustering result (i.e., number of clusters) is based on the fusion of different CVIs. The statistical results showed that the hierarchical MR-DMS outperforms the K-power-means in terms of the probability to estimate the correct number of clusters provided by the WINNER model.

The relation between physical clusters and clusters obtained by high resolution parameter estimation is investigate in Zhu and Tufvesson. [ZT12]. This research work is challenging since the multipath parameter estimators are not directly providing any information on the number of interaction points which the multipath undergoes between the TX and RX. The method used in Zhu and Tufvesson. [ZT12] combines the cluster identification based on a ray launching tool (including a detailed map of the environment) and the clustering results based on the K-power-means. The results show that single bounce (single interaction point) clusters can easily related to physical clusters within the environment. Whereas the physical clusters in the case of multi-bounces are not easy to identify. It is interesting to note that single physical interaction points (scatterer) can simultaneously be part of a single- as well as a multi-bounce cluster. This is in contrast to the COST2100 channel model, where each type of cluster is treated separately. Furthermore, the cluster visibility region, cluster spreads and the cluster selection factor are derived for the considered scenario.

9.5 COST 2100 Channel Model Updates

The COST2100 model is nowadays a well known Geometry-Based Stochastic Channel Model (GSCM). As it was defined in the the previous COST action, COST 2100, there have been further parameterisations of the model for larger range of scenarios and functionality, such as dense multipath, has been added to the publicly available source code. There have also been suggestions for extensions, ideas for further improvements of the model itself or for GSCMs in general. In this section we start discussing some specific considerations on GSCMs and the we review the most important updates to the COST 2100 channel model and channel model implementation.

9.5.1 Scenario Distance

When defining propagation scenarios it is often convenient to refer to the environment where the system is supposed to be used, e.g., indoor office, outdoor-to-indoor, suburban, rural macro cell etc. Often, those propagation

scenarios are further specified by the expected mobility, whether it is a bad or "typical" case, LoS, NLoS etc. However, from a modelling point of view, such an approach may lead to an over-specification of the scenarios, and there migth be cases that from a modelling point of view are very similar, despite their different names. In [NSK15], an objective method to characterise the similarity between large scale parameters of different scenarios and between different measurements in the same scenario was developed. As a similarity metric the authors used the mean Kullback–Laibler divergence, that measures the distance between two distributions. In the special case of two multivariate normal distributions, which is a common case in contemporary channel models such as WINNER and COST2100, the divergence can be calculated as

$$D_{\mathrm{KL}}(P\|Q) = \frac{1}{2\log_e 2}\left[\log_e \frac{\det(\sum_Q)}{\det(\sum_P)} + tr\left(\sum_Q^{-1}\sum_P\right) + (\mu_Q-\mu_P)^T\sum_Q^{-1}(\mu_Q-\mu_P) - k\right], \tag{9.5}$$

where $\sum$ is the $k \times k$ covariance matrix and μ is the mean, respectively, of the multivariate normal distributions P and Q. However, this divergence is not symmetric and therefore the *mean* Kullback–Leibler divergence is used,

$$D_{KL}(P\|Q) = \frac{1}{2}(D_{\mathrm{KL}}(P\|Q) + D_{\mathrm{KL}}(Q\|P)). \tag{9.6}$$

By using the divergence it was concluded that the grouping of the 18 (sub-) scenarios in the WINNER model not always correspond to the smallest distance. With the approach it is possible to, in an objective manner, combine propagation scenarios that from a large scale parameter perspective anyway are quite similar to each other. Similarly, the method can be used as a measure of show close the large scale parameters from a measurement are to the reference scenarios.

9.5.2 Polarisation Characterisation

Polarisation is today included in the major GSCMs like COST 2100 and WINNER models. Typically, the two polarisation states, horizontal (H) and vertical (V), are modelled as independent and thus with independent phases. If slanted polarisations are used, e.g., $\pm 45°e$, the standard cross polarisation ratios alone do not provide information about the ratio between co- and cross polarisation reception; It is important to consider the phase relation between the H and V components as well. The behaviour of polarisation

states for slanted polarisation was investigated in [KyK13]. It was concluded that for outdoor suburban channels it seems that the polarisation state for $\pm 45^{\circ}$ transmission is preserved quite well, whereas circular polarisation has a tendency to have more of an elliptic shape at the RX. For indoor channels, it seems that the polarisation states are quite well preserved for the LoS component, but for the NLoS components the relative phase between the two polarisation states seems to have a more uniform distribution, but it is not completely random. Hence, the WINNER-modelling approach with uniform phase distribution for the NLoS paths and zero phase difference for the LoS path may provide a reasonable approximation, but further work is needed in the area.

9.5.3 Vitual Multi-Link Measurements versus True Multi-Link Measurements

Multi-link communication has become more and more important over the last years, and hence there is a need to capture and characterise the multi-link behaviour in a proper way in measurement campaigns in order to extract, e.g., the joint distributions between different large scale parameters or at least the correlation between them. Ideally, synchronous multi-link measurements should be performed and used for the characterisation, but due to practical limitations this is not always possible. Hence, for static environments repeated measurements along the same route, but with different base station positions, are sometimes used for characterising the multi-link behaviour. The natural question, which was examined in [DFT14b] is though whether both those measurement approaches give the same statistical distributions of the large-scale parameters. For the small-scale behaviour and instantaneous values it is clear that the results of the two approaches give different values, but for the studied static semi-urban microcell scenario the deviation between the results based on the two approaches differed only marginally. No significant difference was found for the multi-link parameters obtained from the synchronous measurements and the repeated measurements, which supports the results in [NKS11].

9.5.4 Cluster Multiplexing

In [DRZ15], a new multiplexing concept was studied, where the aim was to find the probability of having only one user connected to specific cluster, or equivalently a dedicated visibility region for that specific user. The calculated value gives and upper limit of the probability of successfully using directional-based

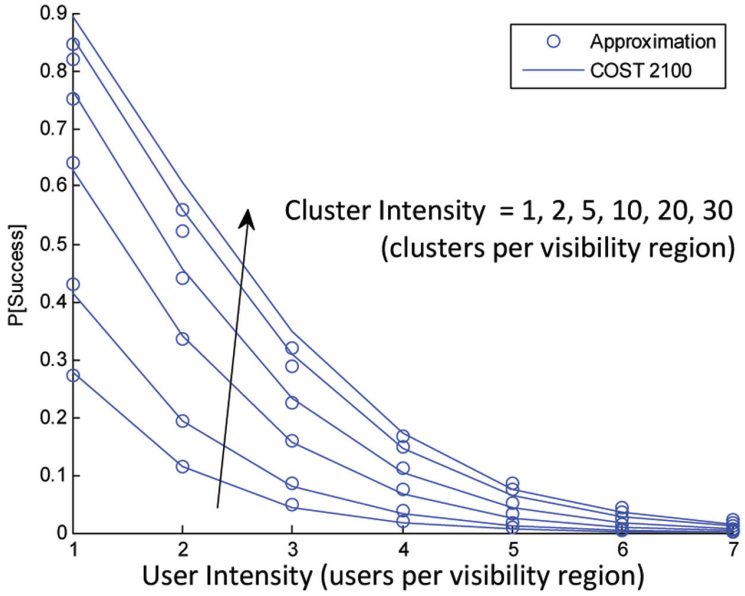

Figure 9.13 The probability of successful cluster multiplexing, i.e., that a specific user has a dedicated cluster.

multiplexing, e.g., beamforming, to communicate with the user of interest give no other collaboration. The main limiting factor for successful reception is the product of the area of the visibility region and the intensity of the users, which in some sense is quite obvious. The probability of successful cluster based multiplexing in a system is close zero when this product is larger than 7.

9.5.5 Physical Clustering

The clusters can often be connected to physical objects in the environment, this is especially true for single bounce clusters. Larger objects in the environment often give rise to a number of MPCs that have similar delay and angular parameters, e.g., a building often have a number of scattering points and therefore contributes with several MCPs to the impulse response. In Zhu et al. [ZHKT14], the concept of physical clusters are introduced and the properties of them are analysed. The physical clusters are extracted based on a measurement-based ray launching tool [ZST12], where the measured estimated MPCs are tracked and visualised in a 3D-map, see Figure 9.14. In this way the interaction points and the interacting objects can be identified and clustering can be performed based on the physical location of the interacting

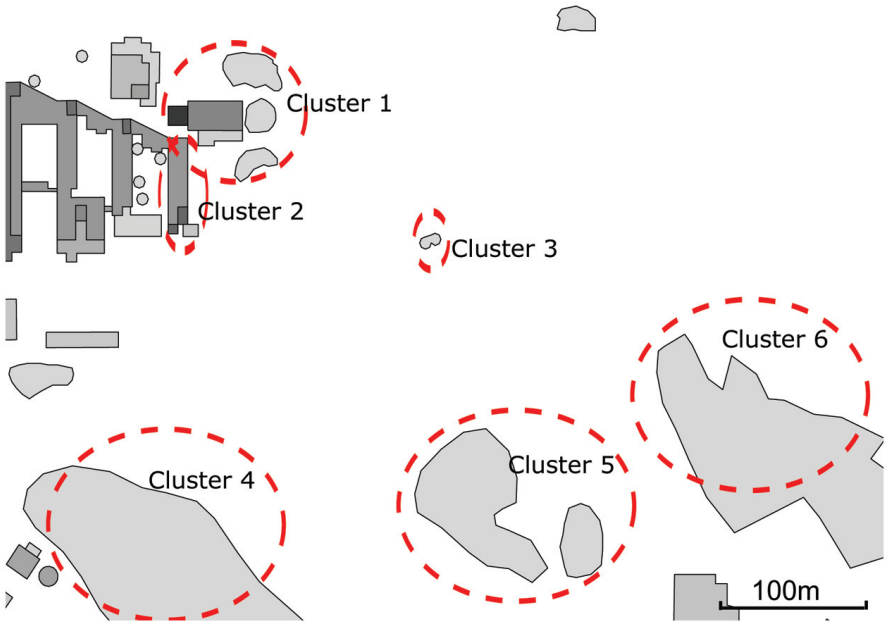

Figure 9.14 Six physical clusters in a sub-urban scenario.

points. The physical clusters show somewhat longer life time (i.e., larger visibility regions) compared to the parmeter-based clusters. They can constitute single-bounce and multiple bounce clusters at the same time, which is not the case for the carameter based clusters. In channel simulations, it was seen that it is somewhat easier to control the delay spread when using physical clusters instead of parameter-based clusters, but the extraction of physical clusters is quite complicated and a more sophisticated physical cluster algorithm is needed in the future. For multi link simulations, the physical cluster approach might be an attractive way forward as the extraction of common clusters to a large extent is based on a physical interpretation of the cluster locations. Parameters for physcial clusters for an sub-urban scenario at 300 MHz and for an urban scenario at 5.3 GHz are given in [Zhu14].

9.5.6 Dense Multipath Component Add On

The propagation of Energy in the radio channel is seen to have two parts: specular components, typically coming from reflections from-large physical objects, and DMCs, that represent the part of the received signal that can

not be resolved in angle and delay. In the COST 2100 model, DMC is represented by many weak Multipath Components (MPCs), each cluster of specular components has a corresponding cluster of DMC, with the same cluster centroid, but with a somewhat larger angular spread and delay spread. In VVirk et al. [VHW14] the implementation of the DMC add on for the COST 2100 model is briefly introduced. The DMC add on is a parallell function to the function generating specular components, the overall structure can be seen in Figure 9.15

9.5.7 Massive MIMO and Distributed MIMO

Massive MIMO is an emerging technology that could enable a significant improvement in data TP, link reliability, and energy efficiency. The key to massive MIMO is to have a large number of antennas at the BS, serving multiple users equipped with rather few antennas, typically one or two. If the antenna array at the BS is physically large, it is important to consider possible variations in the channel characteristics over the array, for example

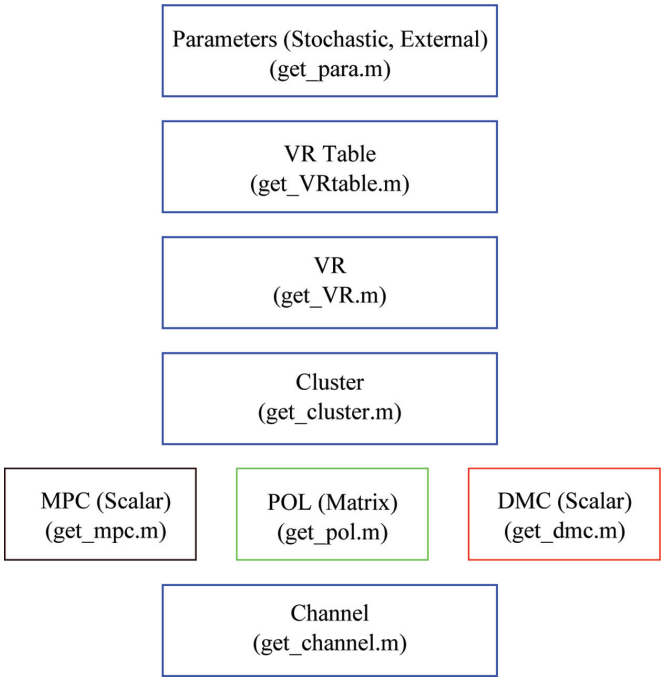

Figure 9.15 Structure of the COST 2100 implementation with the additional DMC function.

with respect to angular spread, delay spread, and large-scale fading, and include such variations in the models in an appropriate way. The COST 2100 channel modelling framework has the advantage that the scatterers in the clusters have a explicit position in the simulation area, hence the effect of spherical wavefronts are implicitly taken care of in the model, which is not the case in, e.g., the WINNER approach. In [Gao16], an extension of the COST 2100 model for massive MIMO was proposed where the concept of visibility regions is applied to the BS side as well. Conventionally, visibility regions for the clusters are applied only on the MS side. By using this concept at the BS side it is possible to let the different BS antennas "see" different clusters, even though they are co-located. By allowing a linearly decreasing or increasing gain function for each visibility region, it is possible to capture and model varying cluster power levels over larger array structures, a property that has been seen in measurements with physically large arrays. A schematic illustration of the BS visibility region concept is shown in Figure 9.16.

Parameters for the BS visibility regions have been extracted from a massive MIMO measurement campaign in Lund, Sweden in a sub-urban NLoS scenario. For each user the total number of clusters that can be seen

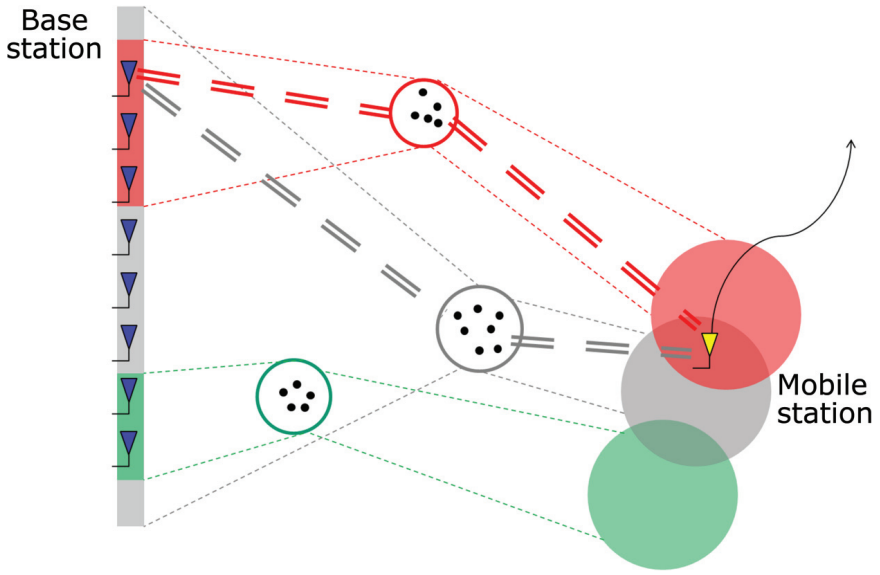

Figure 9.16 Extension of the concept of cluster visibility regions to the base station side. Each cluster has two types of visibility regions: MS-VR and BS-VR.

over the physically large array, in this case a 7.4-m long linear array, can be approximated to follow a negative binomial distribution, the median total number of clusters per user over the array is 10 (r = 2.43 and σ = 0.16 for the negative binomial distribution). The length of the BS visibility regions is modelled as log-normal with median 0.7 m and a standard deviation for the log value of 2. Finally, the slope of the linear (in the dB domain) gain function is modelled as Gaussian with zero mean and standard deviation of 0.9 dB/m for longer visibility regions (above 2 m), whereas the are modelled without a slope for shorter visibility regions.

The influence of the distance between the antennas at the BS side for a massive MIMO or somewhat distributed MIMO setup was investigated in [DFT15]. Especially two-modelling approaches to reflect the fact that the correlation of large scale parameters tend to decrease with increased antenna separation were investigated when a cluster that is created from the same physical object is used for communication. In the first approach, the decorrelation effect was modelled using a power profile for the visibility region, similar to the gain function in [FGD$^+$15], to have an increasing or decreasing power contribution from the different parts of the physical cluster. In the second approach, an observation window that let the BS "see" different parts of the physical cluster was applied. Both methods found to capture the basic behaviour of decreased correlation for increased BS antenna distance and can be used to describe the effects seen in the measurements, the first approach is more consistent with the COST 2100 modelling approach, but further measurements and analysis are needed to validate the approaches.

The high-spatial resolution that is achieved in massive MIMO makes it a good candidate for some tricky scenarios where the used density is high and often under LoS conditions, e.g., during sports events in a stadium or during a concert in an open field or at an arena. To investigate whether massive MIMO has the potential to resolve and separate closely spaced users in LoS conditions, a measurement campaign was conducted and analysed in [FGD$^+$15]. As opposed to the majority of massive MIMO measurement campaigns the measurements were fully synchronous with eight users confined in a circle with a 5-m diameter. It was concluded that the singular value spread in general was low, which is an indication that also the weakest user gets reasonable communication possibilities. The sum-rates achieved through massive MIMO and linear precoding (zero forcing or matched filter precoding) was at the levels of 70–80% of the optimum dirty paper coding capacity, whereas conventional

MIMO schemes fell much shorter attaining 18–34% of the capacity. Also in terms of fairness, it seemed that all users were allocated power while maximising the sum-rates, which is an indication that all the users experienced favourable propagation conditions. All in all, the conclusion was that it seems that massive MIMO is able to reasonably well spatially separate the closely spaced users and provide simultaneous communication possibilities also in the considered scenario, which conventionally is seen as tricky.